Engineering Structures 175 (2018) 425–435

Contents lists available at ScienceDirect

Engineering Structures

journal homepage: www.elsevier.com/locate/engstruct

Behavior and shear strength of steel shape reinforced concrete deep beams

Cheng-Cheng Chen[a], Keng-Ta Lin[b,*], Yu-Jen Chen[a]

[a] Department of Construction Engineering, National Taiwan University of Science and Technology, No. 43, Sec. 4, Keelung Rd, 106 Taipei, Taiwan, ROC
[b] Office of General Affairs, National Kaohsiung University of Sciences and Technology, No. 415, Jiangong Rd., 807 Kaohsiung, Taiwan, ROC

ARTICLE INFO

Keywords:
Steel reinforced concrete beam
Composite construction
Shear strength
Deep beams

ABSTRACT

The shear behavior of steel reinforced concrete (SRC) deep beams was investigated, and an analytical model for predicting the shear strength of SRC deep beams was developed. A total of 12 deep beams were fabricated and tested to failure to study shear behavior. The tests revealed the following: (1) the wide flange shape may contribute considerably to the shear strength of the SRC deep beams; (2) the depth of the wide flange shape may affect the shear strength of the SRC deep beams; and (3) the SRC deep beams possessed more ductile behavior than the RC deep beams did. The softened strut-and-tie (SST) model for predicting the shear strength of RC deep beams was modified to accommodate the effect of wide flange shapes on the shear strength of SRC deep beams. The modified model, called SST-SRC, could capture the shear behavior of the fabricated SRC deep beams.

1. Introduction

Structural members composed of structural concrete, steel reinforcing bars, and structural steel shapes are being used more often recently. In Japan and Taiwan, structures composed of such members are termed steel-reinforced concrete (SRC) structures. Fig. 1 shows a typical cross-section of SRC beams. The procedures for the strength evaluation and design of such beams are quite complicated if the composite action between the steel shape and concrete is considered. Therefore, composite action is usually neglected in the strength evaluation and design of SRC members. Generally, SRC beams do not employ shear connecters, such as shear studs. However, previous test results [1,2] have often shown the obvious composite action of SRC members, even when shear connectors were not employed.

According to the ACI 318-14 code [3], RC beams with a shear span-to-depth ratio (a/h) of less than 2 are defined as deep beams. However, very few codes or provisions [3–6] define SRC beams as SRC deep beams. Both RC and SRC deep beams are characterized by higher shear strength, and the appearance and mechanical behavior of SRC deep beams show many similarities with those of RC deep beams. Thus, in the present study, the RC deep beam classification method is adopted for SRC deep beams.

In Japan, SRC beam research was initiated by Tsuboi et al. [7]. Tsuboi proposed a strength superposition method for determining the shear strength of SRC beams. The a/h of the specimens used in their study was 1.5; therefore, they were classified as deep beams based on the ACI code [3]. Nevertheless, the cross section of the steel shape fabricated using double-angle and steel plates in that study was discontinuous in the span direction, and it differs remarkably from cross sections used in recent constructions. In recent decades, Chen [8] and Weng [2,9] have examined SRC deep beams with an H steel shape, as shown in Fig. 1. Their research has focused on examining the effect of shear studs and vertical shear reinforcements in Taiwan; in addition, the authors have used the concept of superposition to determine the shear strength of SRC deep beams.

The Japanese and Taiwanese codes [5,6] use the concept of strength superposition for the analysis and design of SRC beams; that is, the composite action between the RC and the steel shape is neglected. However, experimental results have shown that the composite action actually exists [2,9], and very few theoretical models have been developed considering composite action. Hwang et al. [10] proposed the softened strut-and-tie (SST) model for determining the shear strength of RC deep beams. The SST model satisfies equilibrium, compatibility, and constitutive laws of cracked RC, and it has provided reasonable estimates of the shear strength of RC deep beams.

Lu proposed an analytical model based on the SST model for predicting the shear strength of SRC deep beams. A total of 16 specimens [2,8,9] have used to verify the model proposed by Lu [11], and the ratios of depth of steel shape d_s over overall depth h were 0.50 and 0.57, respectively. Thus, neither the model proposed by Lu [11] nor the strength superposition method captures the trend of variation in shear strength with the parameter d_s/h. Therefore, investigating the effect of d_s/h on shear strength was a major goal of the present study.

In this study, by means of experimental observation, we

* Corresponding author.
E-mail address: d9005301@mail.ntust.edu.tw (K.-T. Lin).

https://doi.org/10.1016/j.engstruct.2018.08.045
Received 5 February 2018; Received in revised form 10 August 2018; Accepted 15 August 2018

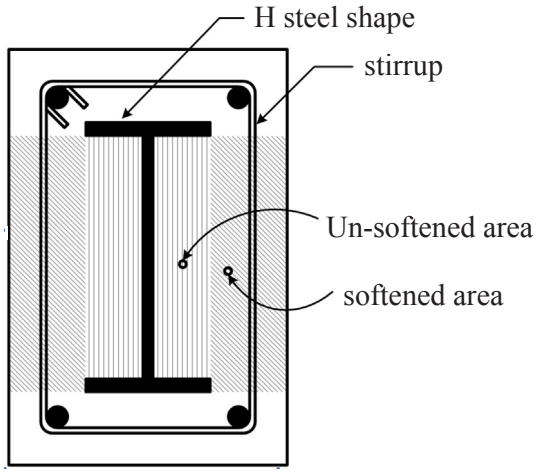

Fig. 1. Typical cross section of an SRC beam.

investigated the shear behavior and composite action of SRC deep beams. Additionally, on the basis of the SST model, we propose an analytical model called SST-SRC model for determining the shear strength of SRC deep beams. The experimental results were used to verify the SST-SRC model and the strength superposition method.

2. Experimental program

2.1. Specimen design and fabrication

A total of 12 full-scale deep beams, comprising 2 RC beams and 10 SRC beams, were designed, fabricated, and tested. Fig. 2 shows the elevation and dimensions of the specimens. All the specimens measured 450 × 550 mm in cross section and 1630 mm in length, as shown in Figs. 2 and 3. The test specimens were simply supported, and the applied load P was equally distributed at Points B and C, as shown in Fig. 2. The 12 specimens were categorized into BRC, B, BI, and BW series, and Table 1 presents the designation and brief descriptions of the specimens.

The specimens in Series BRC, namely. BRC-1 and BRC-2, were two RC specimens having the same dimensions and structural details. Fig. 3(a) shows the cross section of the RC specimens. Eight #10 steel bars were used as longitudinal steel bars, and no transverse steel bars were used.

The specimens in Series B, BI, and BW, as listed in Table 1, were SRC specimens. Regarding the designation of the SRC specimens, the letters before the hyphen stand for the series, and the letters after the hyphen stand for the shape of the steel section employed. The specimens designated B-H2 and BW-H2 were the same specimen belonging to

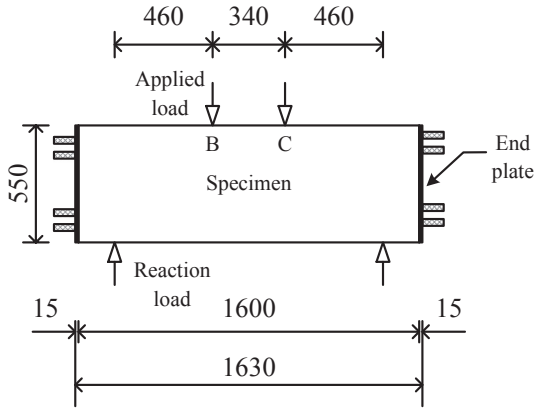

Fig. 2. Overview of specimen (unit: mm).

different series. A total of six different wide-flange steel shapes were used. The designation and the dimensions of the steel shapes are listed and shown in Table 2 and Fig. 3(c), respectively, where d_s is the overall depth, b_f is the flange width, t_w is the web thickness, and t_f is the flange thickness of the steel shape. The centroid of the steel shape coincided with the center of the SRC cross section for all specimens. The arrangement of the steel bars in all SRC specimens was the same as that in the BRC specimens, and it is shown in Fig. 3(a).

Series B comprised four specimens, as presented in Table 1. Each specimen had a different steel shape. Steel shapes H1 to H4 essentially had the same web area A_w, which is defined as the product of d_s and t_w. Consequently, the nominal shear strength of the four wide-flange steel shapes was about the same. However, the depth of the steel shapes varied from 450 to 200 mm, as listed and shown in Table 2 and Fig. 4, respectively.

The four specimens in Series BI were duplicates of the specimens in Series B, except that a layer of lubricant and a layer of plastic paper were applied to the surfaces of the steel shapes to eliminate the bond strength between the steel shapes and the concrete.

Series BW consisted of three specimens, which are presented in Table 1. The steel shapes used in these three specimens had the same depth of 390 mm. However, the thickness of the web varied from 10 to 20 mm.

All specimens, including RC and SRC specimens, had the same arrangement of longitudinal steel bars, as mentioned. Both ends of the steel bars penetrated through the end plates and were connected to the end plates by fillet welds, as shown in Fig. 3(b). None of the specimens contained a transverse steel bar. ASTM A706 steel bars with a measured yield stress f_y of 459 MPa and measured ultimate strength f_u of 651 MPa were used.

The steel shapes were fabricated using ASTM A36 hot-rolled steel shapes and steel plates, as summarized in Table 2. The widths of the flanges of specimens H2, H2A, H2B, and H3 were reduced by cutting off a part of the flange of the original hot-rolled section. The thicknesses of the webs of specimens H2A, H2B, H3, and H4 were increased by welding doubler plates to the web. The thicknesses of the doubler plates t_d are listed Table 2, and the details of the doubler plates are shown in Fig. 3. The measured yield stresses of the webs F_{yw}, doubler plates F_{yd}, and flanges F_{yf} are listed in Table 2 as well. Both ends of the steel shapes were welded to the end plates by fillet welds, as shown in Fig. 3.

A local concrete plant supplied the concrete used in this study, and the average compressive strength of the provided concrete was 40.1 MPa, as determined by conducting load tests.

2.2. Test setup

Fig. 5 shows the test setup. All specimens were loaded monotonically under displacement control by using a universal testing machine with a capacity of 6 MN. A loading beam was used to distribute the applied load P across the specimen through two loading plates, as shown in Fig. 5. The reactions were transmitted to the reaction base through the two loading plates and one steel rod as hinged support at both sides of the specimen. The hinged support is capable of resisting forces acting in any direction of the plane. All loading plates measured 140 mm in width and 550 mm in length. The applied load was measured using the self-equipped load cell of the testing machine, and the deflection at midspan was measured using a linearly variable displacement transducer. The specimens were white washed, and a 100 mm × 100 mm grid was drawn on the front side of the specimens for detecting and recording the crack patterns. The loading tests were terminated as the applied load dropped below 80% of the maximum load reached.